Indian Journal of Science and Technology, Vol 9(36), DOI: 10.17485/ijst/2016/v9i36/102908, September 2016
ISSN (Print) : 0974-6846
ISSN (Online) : 0974-5645

# A Theoretical Analysis of the Dark Current in Quantum Dot Infrared Photodetector using Non-Equilibrium Green's Function Model

**Rahul Kumar Gujral[1]*, V. Damodaran[2] and Kaustab Ghosh[3]**

School of Electronics Engineering, VIT University, Chennai - 600127, Tamil Nadu, India;
rahulgujural254@gmail.com,damodaran.v2013@vit.ac.in,kaustab@vit.ac.in

## Abstract

**Objectives**: This paper entails the theoretical computation of dark current in asgrown and annealed Quantum Dot Infrared Photodetectors (QDIP). **Methods/Statistical analysis:** Here, non-equillibrium Green's function was used to model the dark current characteristics in asgrown and annealed QDIPs. Post-growth thermal annealing, which reduces the traps states in the QD is also simulated using Fick's second law of diffusion. We have developed a self-consistent Poisson's equation solver to compute the potential profile and quasi Fermi level at QD and at the contacts. **Findings:** The theoretically computed dark current obtained from our model is in good agreement with the experimental data, which validates the efficacy of our model. Our computation also predicts decrease in dark current in the QD with increase in annealing temperature at low bias voltage from0.25-1.5 volts. **Application/ Improvements:** Here, we have optimized the dark current for different annealing temperatures for improving the performance of QD device for infrared sensing applications

**Keywords:** Dark Current, Non-Equilibrium Green's Function, Quantum Dot Photodetectors, Theoretical Modeling

## 1. Introduction

Almost over two decades, there have been wide areas of applications where Quantum Dots (QDs) can be used, specifically in the field of optoelectronics devices such as lasers, photodetectors and Infrared (IR) devices[1–5]. The major factor which degrades the performance of the QD photodetectors is due to high generation of dark current, which reduces the device detectivity. Several theoretical researches are carried out for analyzing the dark current in the QD devices[6–9]. However, in most of these approaches the charge particles were treated as semi-classical particles rather than quantum mechanical entities, which fails to describe the transport mechanism in zero-dimensional nanostructures as in QD. Non-Equilibrium Green's Function (NEGF) is a well-known mathematical tool to model the performance of the QD devices in the quantum mechanical domain[10–13]. The advantage of using NEGF model is that phonon-electron scattering at high temperature, non-equilibrium conditions such as application of high bias voltages and interaction from the neighboring lattice can be included in the computation. Hence, in this paper, we present a theoretical model using NEGF formalism to describe the dark current mechanism in the QD. Here, Hamiltonian of the QD system is computed in cylindrical coordinates and semiconductor band-offsets as well as Poisson equation solver was developed to solve for the potential energy of the system for different bias voltages. The Green's function of the system was computed for calculating the local density of states and the dark current. We have also theoretically explored the effect of post growth thermal annealing of the dot which is an effective technique for reducing the trap in the QD and improving the performance. Thus, through this modeling and effect of annealing, we attempt to provide useful information to the device engineers in reducing dark current and fabricate high performance QD photodetectors.

*Author for correspondence

## 2. Theoretical Model and Simulation

For developing our theoretical modeling, we have considered a single layer truncated pyramidal InAs/GaAs QD structure as shown schematically in Figure 1. For computation of Green's function, the QD is considered to be enclosed in a cylinder of radius R and height Z as shown in Figure 2. Since, the average separation between the QDs is considered to be 46 nm, R is taken to be 23 nm. The base diameter of the QD is 14 nm and height of 6 nm. Self-energies are added to the isolated QD system for simulating the coupling between the surrounding contacts and the QD.

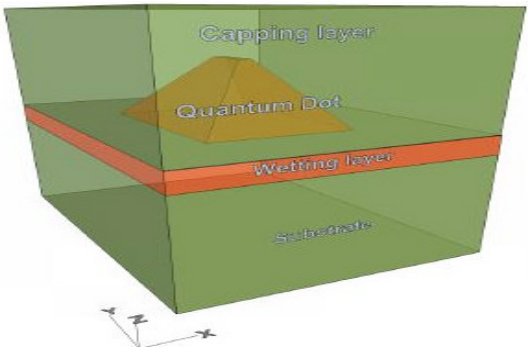


**Figure 1.** Schematic view of the QDIP structures.

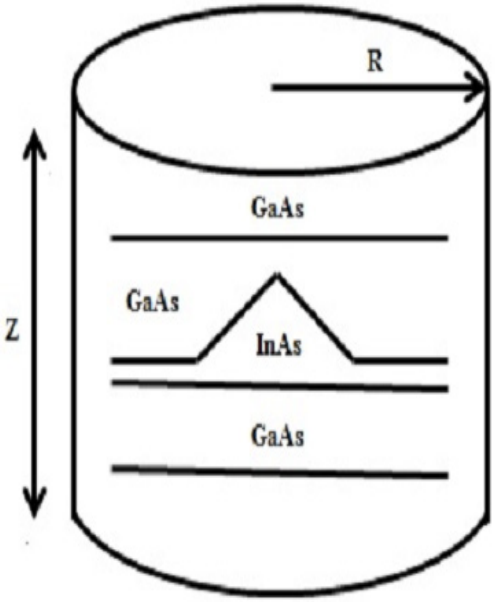


**Figure 2.** Schematic of the QDIP structure in cylindrical coordinates system.

The Hamiltonian of the system is obtained by simulating the potential profile in the QD by incorporating the band-offset of the heterostructure and solving the self-consistent Poisson's equation for the applied bias voltage. Figure 3 depicts the simulated band-offsets obtained due to the difference in band-gap of the InAs and GaAs material forming the QD. We have applied finite difference method for discretizing the Hamiltonian of the QD system and for computation of the Green's function.

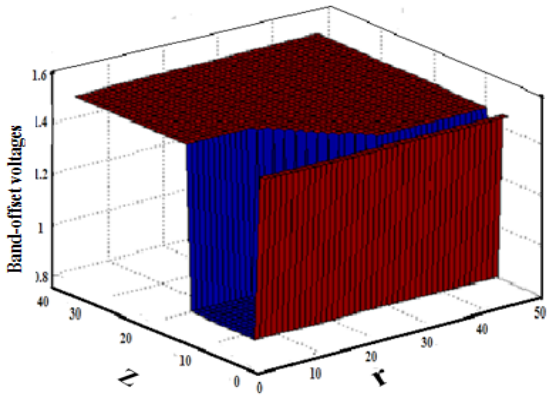


**Figure 3.** Band-offset variations between different heterostructure materials.

### 2.1 NEGF in a Steady State

The retarded green's function in steady state is given by

$$\left[EI - H - \sum^{r} \right] G^{r} = I \tag{1}$$

where, E denotes total energy of the electron, H is the Hamiltonian of the system, $\sum^{r}$ denotes self-energy due to the coupling with the layers and I means identity matrix. In cylindrical representation, the green function is written as:

$$\left[E - H_{op} - \sum_{int}^{r} (r,z;E)\right] G^{r}(r,r';\theta,\theta';z,z';E) = \frac{1}{r}\delta(r-r')\delta(\theta-\theta')\delta(z-z') \tag{2}$$

where $G^{r}$ is the retarded Green's functions and Hamiltonian operator in cylindrical coordinates is written as:

$$H_{op} = -\frac{\hbar^2}{2}\left(\frac{1}{r}\frac{\delta}{\delta r}\frac{r}{m^r(r,z)}\frac{\delta}{\delta r} + \frac{1}{m^r(r,z)} + \frac{\delta}{\delta z}\frac{1}{m^z(r,z)}\frac{\delta}{\delta z}\right)$$

$$+V(r,\theta,z) \quad (3)$$

In Equation (3), $V(r,\theta,z)$ is the potential energy which is seen by an electron and it is given by the sum of the band offsets effective masses respectively.

By replacing the contact layers with self-energy, the equation written as

$$\left[EI - H_n - \sum_n^r \square\right] G_n^r = [r]^{-1} \quad (4)$$

where, $H_n$ means Hamiltonian's matrix representation which is obtained using the method of finite differences. The term r means diagonal matrix. $\sum_n^r \square$ means the self-energy which is obtained by interactions of the leads. The density of states is given by

$$(E) = \frac{1}{2\pi}\int 2\pi r\,dr\,dz\; A(r,z;E) \quad (5)$$

## 2.2 Calculating Self-energy

The scattering and self-energy used in determining the green's functions are due to interactions with the cou

pling of lead. The self-energy is denoted by $\sum^r \square$ and scattering functions is denoted by $(G^< \text{ and } G^>)$. The Hamiltonian used in the Equation (4) is for isolated quantum dot which is replaced by self-energy and it is written as:

$$\sum_n^r \square = \tau[EI - H_{nL}]^{-1}\tau[r_L] \quad (6)$$

where, $\tau$ is called coupling matrix. The elements of the coupling matrix is zero except at the point of interface and the $H_{nL}$ is the Hamiltonian of the contact layer. The self-energy due to the infinite layer of the contact is given by:

$$\sum_{nR}^r \square = t^2 G_{nL}^r R \quad (7)$$

$G_{nL}^r$ means the elements of the green's function

where, t is given by

$$t = \frac{\hbar^2}{2ma^2} \quad (8)$$

t is called hopping parameter and a is lattice grid constant.

The transition rates is given by:

$$\Gamma_n = i\left(\sum_n^r \square - \sum_n^a \square\right) \quad (9)$$

where, $\Gamma_n$ is the transitions rate. Transitions are related to the self-energy.

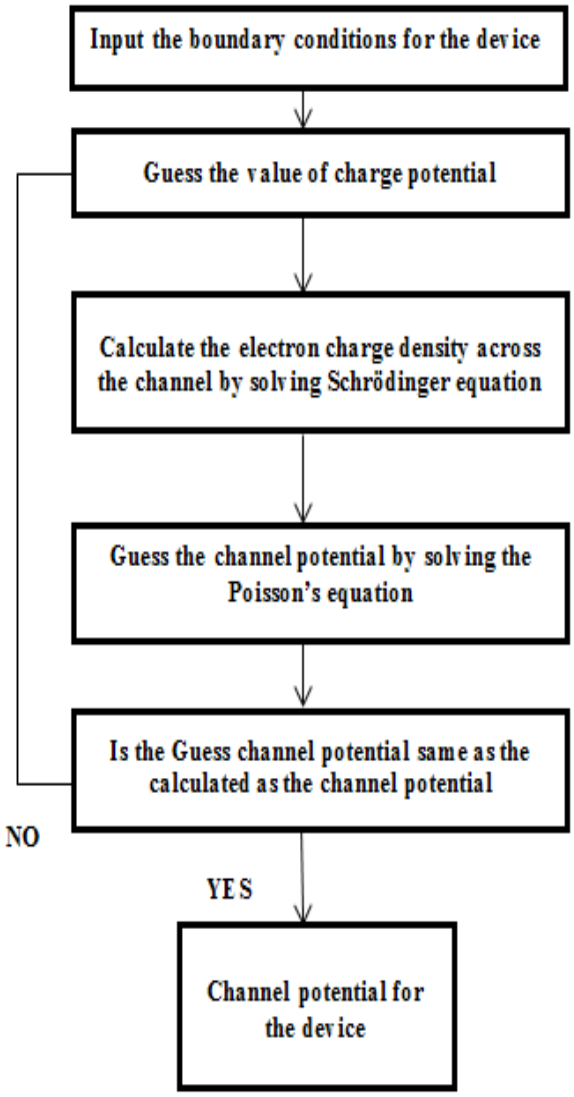


**Figure 4.** Flow chart of the self-consistent Poisson's solver.

The self -energy due to the interaction of leads depends on degree of approximations and type of interac-

tions, which can be elastic or inelastic. For simplicity in our model, we have considered constant internal interaction (electron-electron interaction) which leads to the broadening of the energy levels due to the electron scattering rate. Self-energy due to this internal interaction which we used in our model is given by:

$$\sum_{int}^{r} \square = -i\frac{\hbar}{2\tau_{\varphi}} \tag{10}$$

A self-consistent Poisson's equation is used to determine the average potential in the QD for different bias. It is written as:

$$\frac{d^2U}{dz^2} = \frac{e^2}{\varepsilon}[N_D(z) - n(z)] \tag{11}$$

where, n means electron densities and $N_D$ means doping inside the dots. The flowchart for the overall process is given in Figure 4.

## 2.3 Calculation of Current

The current which is injected from a layers with respective to spectral function which is written as:

$$i_{nL} = \frac{e}{\hbar}Tr\left[\left(-i\sum_{nL}^{<} \square\right)A_n - \Gamma_{nL}(-iG_n^{<})\right] \tag{12}$$

Equation can be applicable to determine the current that present inside the quantum dot cylinder. But with interactions current can be calculated which is written as:

$$i_0(E) = \frac{e}{\hbar}T_n(E)[f_0(E) - f_d(E)] \tag{13}$$

where, $f_0$ and $f_d$ are the Fermi function at the source and the QD respectively.

The total current is given by:

$$I_{\downarrow}0 = \int \square i_{\downarrow}0\ (E)\ \square\ dE \tag{14}$$

The current density of the device is given by

$$J = \frac{I_0}{\pi R^2} \tag{15}$$

Annealing induced inter diffusion in the QD is modeled using Fick's second law of diffusion which is discussed in earlier paper[14].

# 3. Results and Discussion

Our computational result of the density of states for the Asgrown and 750°C annealed QD is presented in Figure 5 (a) and Figure 5 (b) respectively, which exhibits delta-like

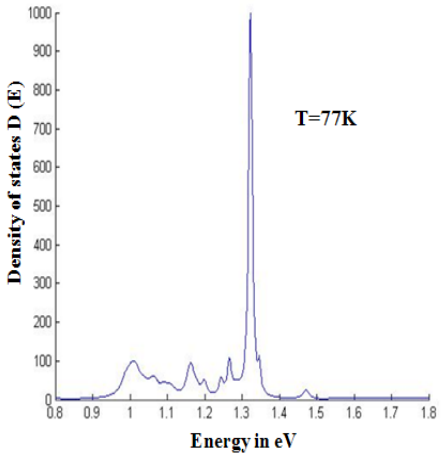


(a)

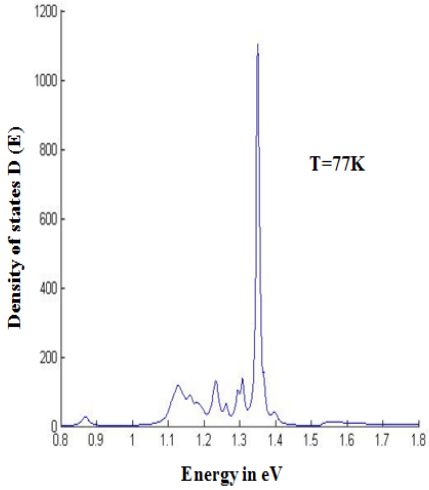


(b)

**Figure 5.** (a) The density of states of the quantum dot at asgrown (b) The density of states of the quantumdot at 750°C annealing sample.

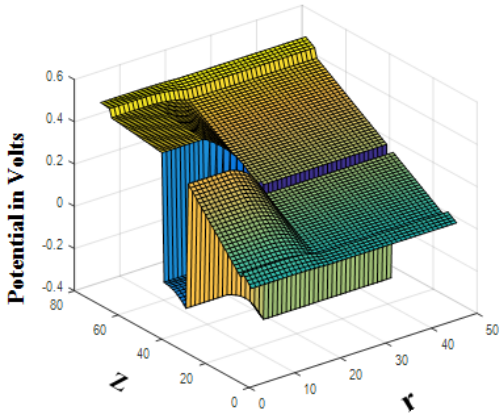


(a)

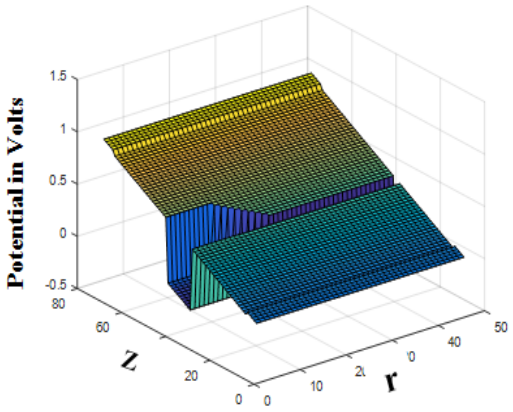


(b)

**Figure 6.** (a) Potential profile for InAs/Ga Asquantum dot at bias voltage of 0.5V (b) Potential profile for InAs/Ga Asquantum dot at bias voltage of 1V.

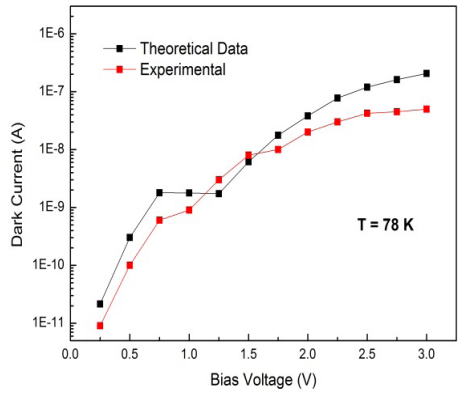


**Figure 7.** Comparison of theoretical data for dark current and with experimental data.

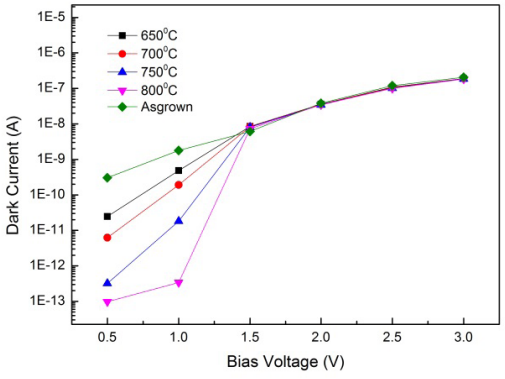


**Figure 8.** Computed values of dark current of the QD for different annealing temperatures.

states at specific quantized energy level. It can be seen that the delta-like states shifts with the increase in annealing temperature. This is attributed to the change in the material composition in the dot due to the annealing induced inter-diffusion resulting in the change in the band structure and the quantized energy states. Figure 6 (a) and Figure 6 (b) shows the simulated potential profile in the QD for different bias voltages which is computed by solving the self-consistent Poisson's equation and the Green's function. It can clearly be seen that with increase in the bias voltage, the potential profile become more slanting, which is due to the larger difference in the quasi Fermi level at the source and at the QD. Thus, more electrons are driven from the source to the QD, resulting in the increase of the dark current. To validate the efficacy of our model, we compared our simulated results with experimental data. The simulation was carried out with the same set of parameters which was used for the experiment. The result is depicted in Figure 7 shows good agreement with the experimental data at low bias voltages. However, a slight deviation at higher bias voltage is observed i.e. the simulated data predicted higher $10^{-7}$ A higher dark current than which is obtained by the experiment. A probable reason for this deviation might be due to the electron-electron scattering effects which is more prominent at higher voltages. It is expected to have reduced electron -phonon scattering in QDIPs due to phonon bottleneck effect. However, incorporation of electron phonon interaction in our model could impart a better match with the experiment even at higher voltages, which is computationally intensive. Figure 8 shows the computed dark current in the QD for different annealing temperatures. It can be observed that with increase is annealing temperature, there is a substantial decrease in the dark current at lower bias voltages from 1.5 - 0.25 Volts. This phenomenon can be attributed to the passivation of defects and trap states with annealing leading to higher carrier confinement[15–17]. However, at higher voltages, we presume that the carriers in the traps are driven out with the increasing field in the asgrown QD. Hence, traps are discharged in the asgrown QD at higher bias voltage. This results in the same order dark current for asgrown and annealed QD for bias voltage exceeding 1.5 Volts.

## 4. Conclusions

In this work, we have presented a detailed theoretical model using non-equilibrium Green's function for eluci-

dating the carrier dynamics in the QD and generation of dark current. Simulation based on post-growth annealing and its impact on dark current characteristics at different bias voltages is also studied. Our findings revealed decrease in the dark current with increase in annealing temperature at bias voltages from 0.25 to 1.5 volts, implying reduction of traps states in the QD and improving the carrier confinement. This study thus also sheds light on the effects of annealing in QDs, which can be used to optimize and reduce the undesirable dark current and improve the overall device performance.

## 5. Acknowledgement

Author KG acknowledges the financial assistance from DST, govt. of India, through a project, for this work. Authors would like to thank the anonymous reviewers for their comments in improving the paper and also we extend our gratitude to VIT University, Chennai for their support.

## 6. References

1. Ledentsov NN, Grundmann M, Heinrichsdorff F, Bimberg D, Ustinov VM, ZhukovA E, Maximov MV, Alferov ZI, Lott JA. Quantum-dot heterostructure lasers. IEEE Journal of Selected topics in Quantum Electronics. 2000 May; 6(3):439–451.
2. Bimberg D. Quantum dot for lasers, amplifiers and computing. Journal of Physics D: Applied Physics. 2005 Jun; 38(13):2055–8.
3. Liu HC. Quantum dot infrared photodetectors.bOpto-Electronics Review. 2003; 11(1):1–5.
4. Maimon S, Finkman E, Bahi rG, Schacham SE, Garcia JM, Petroff PM. Inter sublevel transitions in InAs/GaAs quantum dots infrared photodetectors. Applied Physics Letters. 1998 Jul; 73(14):2003–5.
5. SaiChaitanya BVS, Sekhar TC, Ramesh NVK. IOT based Smart IR device using CC3200. Indian Journal of Science and Technology. 2016 Apr; 9(16):1–5.
6. Ryzhi V. The theory of quantum-dot infrared phototransistors. Semiconductor Science Technology. 1996; 11:759–65.
7. Ryzhi V, Pipa V, Khmyrova I, Mitin V, Willander M. Dark current in quantum dot infrared photodetectors. Japan Society Applied Physics. 2000 Dec; 39:L1283–5.
8. Bhattacharya P, Su XH, Chakrabarti S, Ariyawansa G, Perera AGU. Characteristics of a tunneling quantum-dot infrared photodetector operating at room temperature. Applied Physics Letters.2005 May; 86(19).
9. Stiff-Roberts AD, Su XH, Chakrabarti S, Bhattacharya P. Contribution of field-assisted tunneling emission to dark current in InAs-GaAs quantum dot infrared photodetectors. IEEE Photonics Technology Letters. 2004 Mar; 16(3):867–9.
10. Naser MA, Deen MJ, Thompson DA. Theoretical modeling of dark current in quantum dot infrared photodetectors using non-equilibrium Green's functions. Journal of Applied Physics. 2008 Jul; 104(1).
11. Naser MA, Deen MJ, Thompson DA. Photocurrent modeling and detectivity optimization in resonant tunneling quantum dot infrared photodetector. IEEE Journal of Quantum Electronics. 2010 Jun; 46(6):849–59.
12. Tavakoli SG, Naser MA, Thompson DA, Deen MJ. Experimental characterization and theoretical modeling of the strain effect on the evolution and inter-band transitions of InAs quantum dots grown on $I^{n_x}Ga_{1-x}As$ metamorphic pseudo subtrates on GaAs wafers. Journal Applied Physics. 2009 Sep; 106(6).
13. Naser MA, Deen MJ, Thompson DA. Spectral function of InAs/InGaAs quantum dot in a well detector using Green's functions. Journal Applied physics. 2006 Dec; 100(9).
14. Ghosh K, Naresh Y, Reddy NS. A Theoretical investigation on the dimensions and annealing effects of InAs/GaAs quantum dots for device applications at high bit-rate optical transmission window of 1.3–1.55 μm. Advanced Materials Research. 2012 Oct; 584:423–7.
15. Yang T, Nishioka M, Arakawa Y. Optimizing the GaAs capping layer growth of 1.3um InAs/GaAs quantum dots by a combined two-temperature and annealing process at low temperatures. Journal of Crystal Growth .2008 Dec; 310(24):5469–72.
16. Perret N, Morris D, Franchomme L, Cote R, Fafard S, Aimez V, Beanvais J. Origin of inhomogeneous broadening and alloy intermixing in InAs/GaAs self-assembled quantum dots. Physical Review B. 2000 Aug; 62(8).
17. Leon R, KimY, Jagadish C, Gal M, Zou J, Cockayne DJH. Effect of inter diffusion on the luminescence of InGaAs/GaAs quantum dots. Applied Physics Letters.1996 Jul; 69(13).